Adsorption of CO_2, CH_3OH, and H_2O on Fe(III)-Substituted Calcium Hydroxyapatites

Tatsuo Ishikawa,* Hiroshi Saito, Akemi Yasukawa, and Kazuhiko Kandori

School of Chemistry, Osaka University of Education, 4-698-1 Asahigaoka, Kashiwara, Osaka 582

(Received September 18, 1995)

Calcium hydroxyapatites (CaHAP) substituted with Fe^{3+} ions of different atomic ratios $Fe/(Ca+Fe)=X_{Fe}$ from 0 to 0.23 were synthesized and characterized by various methods. The number of Ca^{2+} ions in CaHAP substituted by one Fe^{3+} ion was higher than one, implying that the formation of cation vacancies and the protonation of PO_4^{3-} ions are caused by Fe(III)-substitution. X_{Fe} of the surface layer of the particles determined by XPS was less than the total X_{Fe}. IR spectra of Fe(III)-substituted CaHAP contain a band at 3707 cm^{-1} assigned to the surface Fe–OH groups in addition to the surface P–OH bands at 3688, 3677, and 3658 cm^{-1}. With an increase in X_{Fe}, the amount of irreversible adsorption of CO_2 decreased whilst those of CH_3OH and H_2O first decreased and then increased. IR results showed that the surface Fe–OH groups act as stronger irreversible adsorption sites for CO_2 and CH_3OH compared to the surface P–OH groups.

Calcium Hydroxyapatite $Ca_{10}(PO_4)_6(OH)_2$ (CaHAP) is not only the main component of biological hard tissue but also an adsorbent for biomaterials such as proteins and a catalyst for decomposition of alcohols.[1] Understanding of the surface structure and nature of CaHAP is fundamentally important for utilizing this material as an adsorbent or a catalyst. The Ca^{2+} ions of CaHAP can be easily replaced with various metal ions and there have been many studies of the ion-exchange behavior of CaHAP in the aqueous phase.[2—8] However, only a few investigations on the surface structure of CaHAP doped with metal ions have been reported except for some studies of the catalytic properties. Misono and Hall[9] have studied the oxidation–reduction properties of Cu(II)- and Ni(II)-substituted CaHAP by EPR spectroscopy and suggested that the surface Cu^+ ions formed by reduction of the surface Cu^{2+} ions are the active sites for the H_2–D_2 exchange reaction. Recently, Matsumura et al.[10] have reported that the oxidative coupling of methane to ethane and ethene can be effectively catalyzed over Pb(II)-substituted CaHAP and that the surface Pb^{2+} ions activate methane and stabilize methyl radicals. However, the detailed surface structure of CaHAP doped with these metal ions still remains unclear.

We have studied the surface structure of different hydroxyapatites (HAP) such as CaHAP,[11—14] strontium hydroxyapatite (SrHAP),[15] and solid solutions of CaHAP and SrHAP[16] by IR spectroscopy and found that the surface P–OH groups on these HAPs are the adsorption sites for H_2O,[11] CH_3OH[13] and CH_3I.[13] Furthermore, we have found that the state of the surface P–OH groups and the adsorption of CO_2 depend on the kind of cations and the stoichiometry of these HAPs.[14—16] We expected that the exchange of Ca^{2+} ions of CaHAP with trivalent cations such as Fe^{3+} ions may cause more pronounced change of the surface structure and the nature of CaHAP compared to the exchange with Sr^{2+} ions.

This study was conducted to clarify the influence of Fe(III)-substitution on the surface structure and the nature of CaHAP. The CaHAP particles doped with different amounts of Fe^{3+} ions were prepared and characterized by various techniques. The adsorption sites for CO_2, CH_3OH, and H_2O on Fe(III)-substituted CaHAP are discussed on the basis of the obtained results.

Experimental

Materials. The CaHAP particles doped with Fe^{3+} ions of different atomic ratios Fe/(Ca+Fe) from 0 to 0.23 were synthesized by the wet method used for preparing CaHAP.[11] The reagents, 0.36—0.40 mol $Ca(OH)_2$ and 0—0.04 mol $FePO_4$, at the total mole number of 0.4, were added to 20 dm^3 of deionized and distilled water free from CO_2 in a capped Teflon container and stirred for 1 d at room temperature. Although $Ca(OH)_2$ was not completely dissolved by this stirring, 0.166 mol of H_3PO_4 were added to the suspension. The suspensions were aged in a sealed container at 373 K for 48 h. The pH of the suspensions after the aging decreased from 7.49 to 5.22 as the amount of $Ca(OH)_2$ decreased from 0.40 to 0.36 mol. After the aging the precipitates were filtered, washed with 5 dm^3 of deionized distilled water and finally dried at 343 K for 1 d. The washing was sufficient to give the surface free from impurities as confirmed by the FTIR spectroscopy.

Characterization. The materials thus obtained were characterized by various methods as follows. Powder X-ray diffraction (XRD) was performed using a Rigaku diffractometer with a Ni-filtered $K\alpha$ radiation at 15 mA and 30 kV. Morphology of the particles was observed using a JEOL transmission electron microscope (TEM). Thermogravimetry (TG) curves of 10 mg samples were measured in air at a heating rate of 5 K min^{-1} using a Seiko thermoanalyzer with a sensitivity of 10 μg employing Al_2O_3 as a reference sample. To study the surface structure of the materials, IR spectra were measured in situ using a Digilab Fourier-transform near infrared (FTNIR) spectrometer with a PbSe detector having a high sensitivity above 2000 cm^{-1}. Samples for FTNIR, pressed into the self-supporting disks with a diameter of 1 cm, were out-

gassed in a vacuum cell at 573 K for 2 h. In order to determine the chemical composition and the state of Fe^{3+} ions in the surface layer of the materials, X-ray photoelectron spectroscopy (XPS) was carried out using a Shimadzu photoelectron spectrometer. Ca and Fe contents were determined with a Seiko inductively coupled plasma spectrometer (ICP) by dissolving the material in a 12 mol dm^{-3} HCl solution and PO_4^{3-} ions were assayed colorimetrically by the molybdenum blue method.[17] The specific surface area was estimated by the BET method from N_2 adsorption isotherms measured at the boiling temperature of liquid N_2 using an automatic volumetric apparatus designed in our laboratory. The samples were pretreated by outgassing at 573 K for 2 h to remove adsorbed water.

Adsorption of CO_2, CH_3OH, and H_2O. Adsorption isotherms of CO_2 were measured at 298 K using the same volumetric equipment for N_2 adsorption. Isotherms of CH_3OH and H_2O were determined at 298 K using an automatic gravimetric apparatus capable of measuring the adsorption isotherm at a wide pressure range from 10^{-4} Torr (1 Torr = 133.3 Pa) to the saturated pressure of the adsorptives. The isotherms at a low pressure range are useful to get the information of adsorbate–adsorbent interaction in the initial stage of adsorption. The number of data of each isotherm was about 100. Before adsorption the samples were outgassed at 573 K for 2 h. To know the adsorption sites for CO_2 and CH_3OH, IR spectra were measured in situ using FTNIR with a vacuum cell. The temperature of the samples in the cell was controlled at 298 K and the heating of the samples by IR ray was minimized by using IR beam less than 6 mm in diameter.

Results and Discussion

Structure of Fe(III)-Substituted CaHAP. Figure 1 depicts the XRD patterns of CaHAP doped with different amounts of Fe^{3+} ions, which show only the diffraction peaks characteristic of CaHAP, although the crystallinity of the materials reduces with an increase in amount of Fe^{3+} ions. The crystallite sizes, obtained by the Scherrer equation from the diffraction peak due to the (002) and (100) planes, are plotted against the atomic ratio Fe/(Ca+Fe) (abbreviated X_{Fe}) of the materials by the open marks in Fig. 2. Taking into account an error of ca. 10 nm for the crystallite size and an error of less than 1% for X_{Fe}, the crystallite size (the squares) obtained from the (100) plane decreases with increasing X_{Fe}, but that (the circles) from the (002) plane shows a maximum at $X_{Fe} = 0.04$.

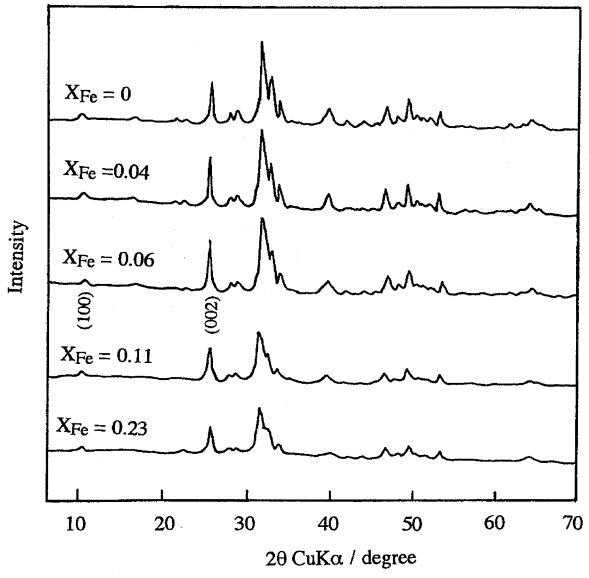

Fig. 1. XRD patterns of CaHAP substituted with Fe^{3+} ions at different X_{Fe}.

Figure 3 displays the TEM pictures of the CaHAP particles doped with varied X_{Fe}. From observing these pictures the pure CaHAP particles are rod-shaped with a mean size of 50 nm (length) and 10 nm (width) and the particle width decreases and the particle length increases as X_{Fe} increases. The particles ($X_{Fe} = 0.23$) contain amorphous particles in addition to the rod-shaped particles, so that the samples with $X_{Fe} = 0$—0.11 were selected for later experiments. The specific surface area of CaHAP doped with different X_{Fe} is plotted against X_{Fe} by the filled circles in Fig. 2. The surface area increases with an increase in X_{Fe}. The *t*-plot[18] of the N_2 adsorption isotherms showed that none of the materials are microporous.

XPS spectra of Fe(III)-substituted CaHAP were taken in order to characterize the surface layer of the particles. The spectra of the samples with different X_{Fe} are shown in Figs. 4 and 5. As seen in Fig. 4 the peak of $Fe2p_{3/2}$ appears at 711.5 and 712.1 eV for the samples with $X_{Fe} = 0.06$ and 0.11, respectively and this peak grows as X_{Fe} increases, while the sample ($X_{Fe} = 0.04$) shows no clear peak. The peaks of $Ca2p_{1/2}$ and $Ca2p_{3/2}$ of pure CaHAP shown in Fig. 5 are observed at 351.0 and 347.5 eV, respectively. The intensities of these peaks decrease with a slight peak shift to a high binding energy as X_{Fe} increases. Mcintyre and Zetaruk have reported that the $Fe2p_{3/2}$ peaks of FeO, Fe_2O_3, Fe_3O_4, and FeOOH appear respectively at 709.2, 710.7, 711.0, and 711.6 eV.[19] The $Fe2p_{3/2}$ peak of Fe(III)-substituted CaHAP is closest to that of FeOOH among these iron oxides, implying that Fe^{3+} ions doped into CaHAP exist as Fe^{3+} ions coordinated by O atoms and OH^- ions. The atomic percents of Fe, Ca, P, and O and the atomic ratios Fe/(Ca+Fe) and (Ca+Fe)/P in the surface

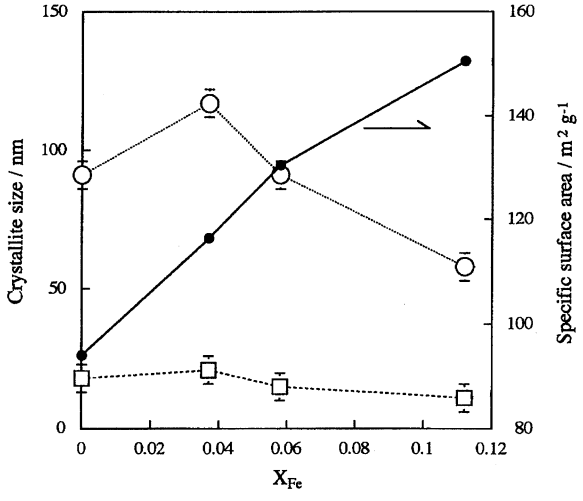

Fig. 2. Crystallite size and specific surface area vs. X_{Fe}. ○, crystallite size determined from (002) plane; □, crystallite size determined from (100) plane; ●, specific surface area.

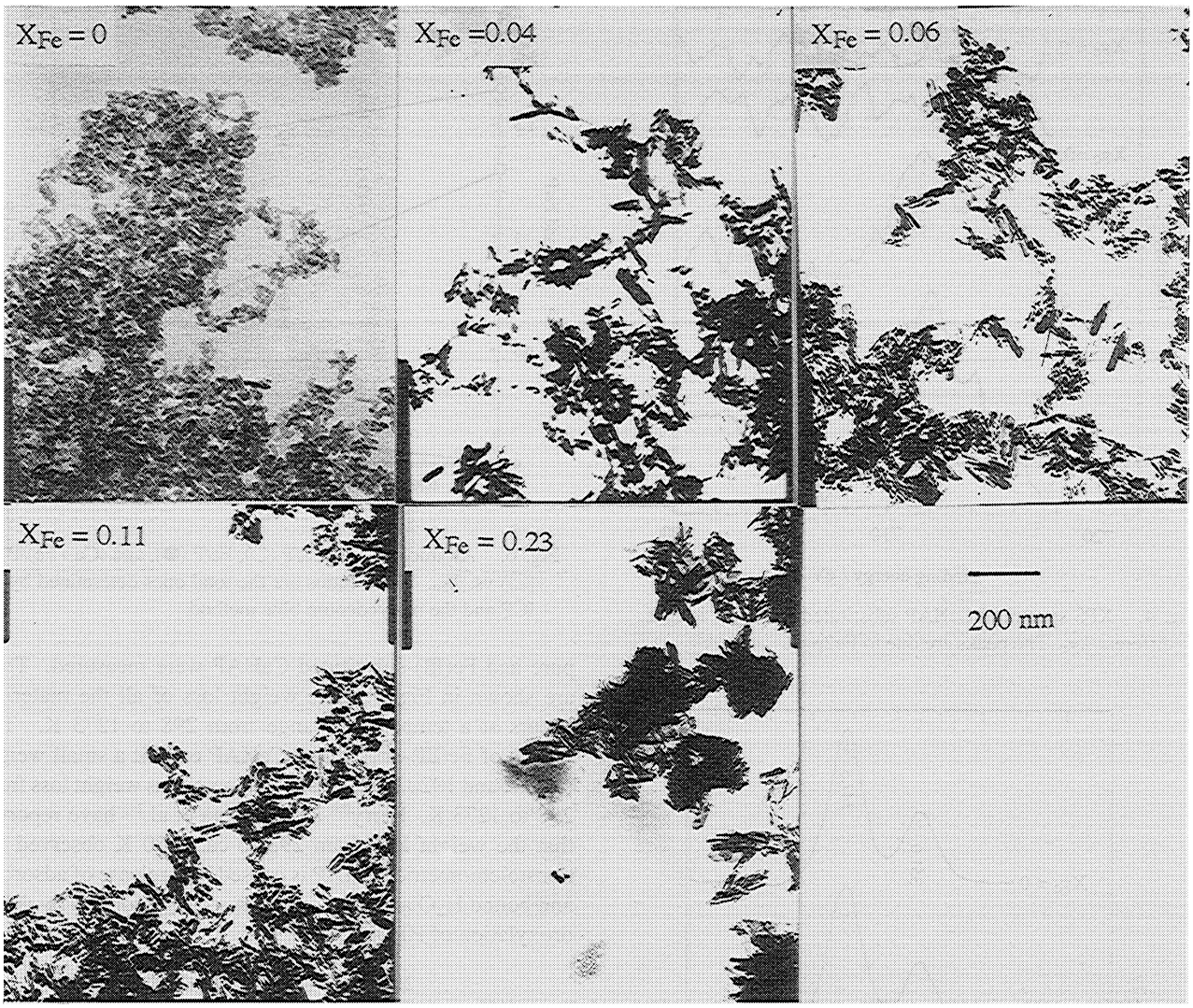

Fig. 3. TEM pictures of CaHAP substituted with Fe^{3+} ions at different X_{Fe}.

layer of the particles, estimated from the area intensity of the XPS peaks, are shown in Table 1 along with the total atomic ratios of the particles obtained by ICP and the molybdenum blue method. Note that the surface Fe/(Ca+Fe) determined by XPS is extremely less than the total one. The surface and total (Ca+Fe)/P ratios of pure CaHAP are identical while in the case of Fe(III)-substituted CaHAP the surface ratio is larger than the total one. These results reveal that the surface composition of Fe(III)-substituted CaHAP differs from the bulk one. However, further quantitative discussion on the surface composition is difficult owing to a high noise in the XPS spectra as shown in Fig. 4.

Table 1. Surface Composition of Fe(III)-Substituted CaHAP Determined by XPS

Atom/%				Atomic ratio			
Fe	Ca	P	O	$\frac{Fe}{(Ca+Fe)}$	$\frac{(Ca+Fe)}{P}$	$\frac{Fe}{(Ca+Fe)}$ a)	$\frac{(Ca+Fe)}{P}$ a)
0	24.1	14.5	61.4	0	1.66	0	1.66
0	23.9	13.0	63.1	0	1.84	0.04	1.64
0.3	23.4	12.6	63.7	0.01	1.86	0.06	1.54
0.4	21.5	13.8	64.3	0.02	1.56	0.11	1.50

a) The total ratios determined by ICP and the molybdenum blue method.

Figure 6 shows the total atomic ratios Ca/P, Fe/P, and (Ca+Fe)/P determined by ICP and the molybdenum blue method as a function of X_{Fe}. With increasing X_{Fe}, the Ca/P ratio (the open circles) decreases and the Fe/P ratio (the filled circles) increases, which demonstrates that Ca^{2+} ions in CaHAP are exchanged with Fe^{3+} ions. The exchange ratio Ca/Fe which is the number of Ca^{2+} ions substituted by one Fe^{3+} ion can be estimated by dividing the slope of the straight line for Ca/P by that of the straight line for Fe/P. The exchange ratio thus estimated is 1.6±0.6, i.e., greater than one, signifying that more than one Ca^{2+} ion are replaced with one Fe^{3+} ion. Therefore, Fe(III)-substitution should produce cation vacancies and cause protonation of the neighboring PO_4^{3-} ions to maintain the total charge balance. The formation of cation vacancies is supported also by the result shown in Table 1 that the total (Ca+Fe)/P decreases from 1.66 to 1.50 with an increase in X_{Fe} and these ratios

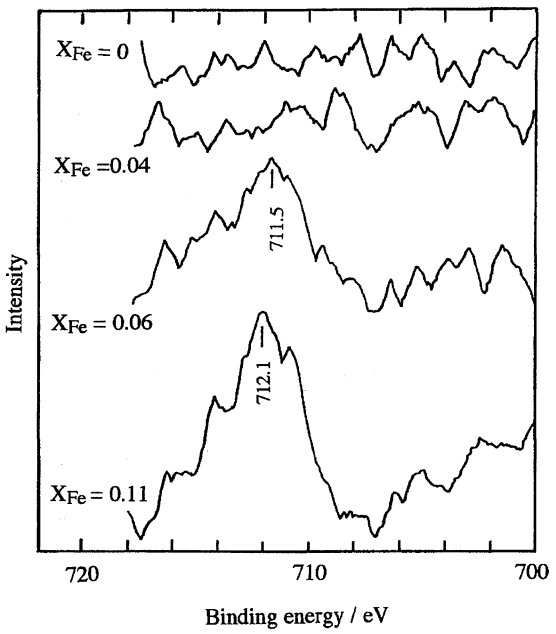

Fig. 4. XPS spectra of CaHAP substituted with Fe^{3+} ions at different X_{Fe}. The peaks are due to $Fe2p_{3/2}$.

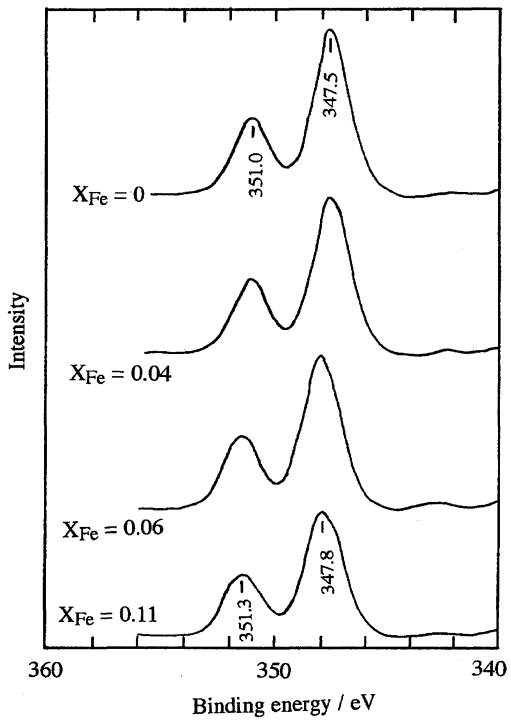

Fig. 5. XPS spectra of CaHAP substituted with Fe^{3+} ions at different X_{Fe}. The peaks are due to $Ca2p_{1/2}$ and $Ca2p_{3/2}$.

are less than the stoichiometric cation/P ratio (1.67). On the other hand, the surface (Ca+Fe)/P increases with Fe(III)-substitution to be more than 1.67. These findings suggest that the surface composition is rather different from the bulk one.

To confirm the protonation of PO_4^{3-} ions and the formation of cation vacancies by Fe(III)-substitution, TG curves of

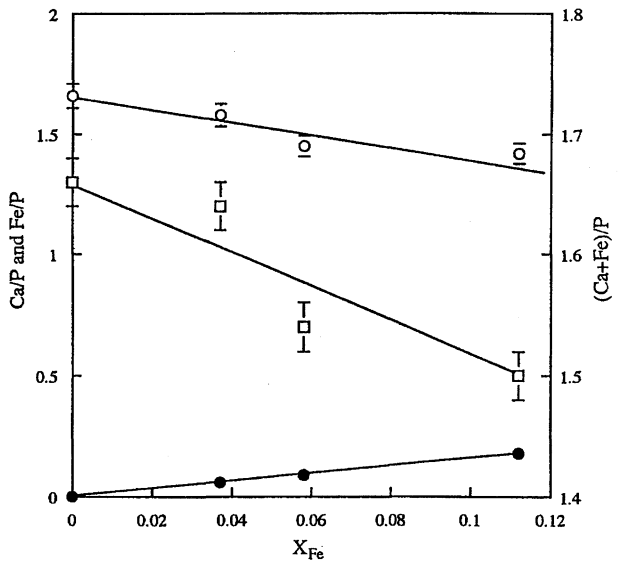

Fig. 6. Atomic ratios of Ca/P (○), Fe/P (●), and (Ca+Fe)/P (□) vs. X_{Fe}. These ratios are the total ones determined by ICP and the molybdenum blue method.

pure and Fe(III)-substituted CaHAP were measured. They are shown in Fig. 7. The weight loss of all the materials occurs at a temperature range from 298 to 1273 K. The curves of Fe(III)-substituted CaHAP exhibit a small weight loss around 1020 K besides the monotonous weight loss from 298 to 1273 K. Berry[20] and Monma et al.[21] have reported that the weight loss from 298 to ca. 1000 K observed for nonstoichiometric CaHAP is caused by a release of adsorbed and bound H_2O and small amounts of H_2O formed by dehydroxylation of HPO_4^{2-} ions:

$$2HPO_4^{2-} \longrightarrow P_2O_7^{4-} + H_2O. \quad (1)$$

The smaller weight loss near 1020 K is due to the reaction of

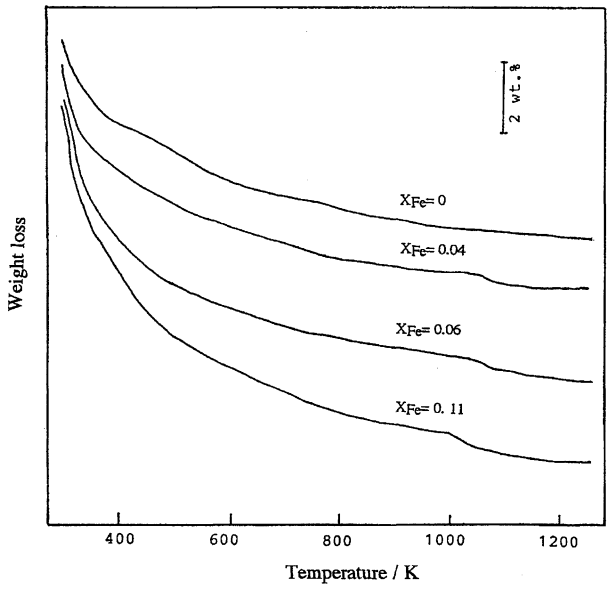

Fig. 7. TG curves of CaHAP substituted with Fe^{3+} ions at different X_{Fe}.

the $P_2O_7^{4-}$ ions formed by reaction (1) with the lattice OH^- ions:

$$P_2O_7^{4-} + 2OH^- \longrightarrow 2PO_4^{3-} + H_2O \quad (2)$$

As seen in Fig. 7, pure CaHAP ($X_{Fe}=0$) with a Ca/P ratio of 1.66 close to the stoichiometric ratio (1.67) shows extremely small weight loss near 1020 K, meaning that this CaHAP possesses essentially no HPO_4^{2-} ions. However, as described below, IR spectrum of this pure CaHAP (Fig. 8) has the bands due to the surface P–OH groups. This is indicative of the existence of HPO_4^{2-} ions having P–OH group in stoichiometric CaHAP, in conflict with the TG result suggesting the absence of HPO_4^{2-} ions in pure CaHAP with Ca/P=1.66 close to the stoichiometric ratio. This discrepancy would be explained by a possibility that the amount of surface HPO_4^{2-} ions is not sufficient to be detected by TG or that the dehydroxylation process of surface HPO_4^{2-} ions differs from that of bulk ones. Both the weight loss between 298 and 1273 K and the weight loss around 1020 K increase as X_{Fe} increases. Hence the weight loss of Fe(III)-substituted CaHAP is caused by a removal of physically and chemically adsorbed H_2O, H_2O produced in reactions (1) and (2) and H_2O formed by dehydroxylation of surface HPO_4^{2-} ions, as confirmed by FTNIR spectroscopy.

Surface Structure of Fe(III)-Substituted CaHAP. For the surface characterization of Fe(III)-substituted CaHAP, IR spectra of the samples outgassed at different temperatures were recorded. Figure 8 illustrates the spectra of the samples outgassed at 573 K for 2 h. The spectrum for pure CaHAP ($X_{Fe}=0$) shows the absorption bands at 3688, 3677, and 3658 cm^{-1}, which have been assigned to the O–H stretching mode of surface P–OH groups.[11] These surface P–OH groups are formed by protonation of the surface PO_4^{3-} ions to compensate not only the charge imbalance caused by cations vacancies but also the surface charge due to unsaturated bonding of the surface PO_4^{3-} ions. As shown in Fig. 8, the spectrum of pure CaHAP ($X_{Fe}=0$) with Ca/P of 1.66 close to the stoichiometric ratio (1.67) has surface P–OH bands, suggesting that the surface P–OH groups are formed mainly to balance the surface charge. With increasing X_{Fe} the 3677-cm^{-1} band grows and the 3688-cm^{-1} band diminishes, that is, the state of the surface P–OH groups varies with Fe(III)-substitution.

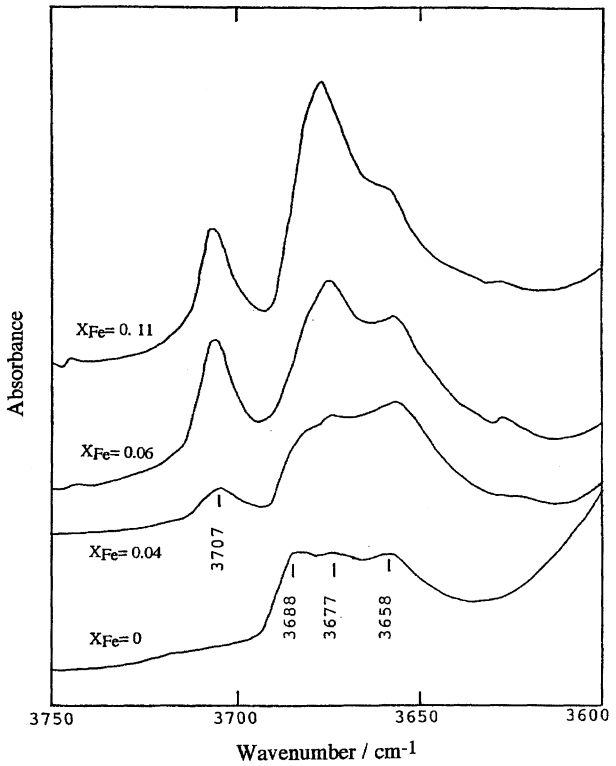

Fig. 8. IR spectra in vacuo of CaHAP substituted with Fe^{3+} ions at different X_{Fe}.

IR spectra of Fe(III)-substituted CaHAP (Fig. 8) exhibit a new band at 3707 cm^{-1} in addition to the surface P–OH bands. This new band completely disappeared when outgassed above 673 K, while the surface P–OH bands were lowered at elevated outgassing temperature but still observed at 773 K. To assign the 3707-cm^{-1} band, we examined the H–D exchange by repeating adsorption and desorption of heavy water. The 3707-cm^{-1} band disappeared and a band appeared at 2733-cm^{-1} after this exchange, and the wavenumber ratio of these two bands was 1.356 close to the theoretical isotope ratio ($\nu_{OH}/\nu_{OD}=1.374$). Therefore, the 3707-cm^{-1} band can be assigned to the stretching mode of surface OH groups. The Fe^{3+} ions replacing the surface Ca^{2+} ions binding to OH^- ions would produce surface Fe–OH groups. Moreover, the wavenumber of this band is near to 3773—3659 cm^{-1} due to the surface free Fe–OH bands observed for β-FeOOH.[22] Consequently, we can assign the 3707-cm^{-1} band to the O–H stretching mode of the surface Fe–OH groups.

Adsorption of CO_2, CH_3OH, and H_2O on Fe(III)-Substituted CaHAP. Figure 9 compares adsorption isotherms of CO_2 on pure and Fe(III)-substituted CaHAPs. The second isotherms (the open marks) were determined on the samples outgassed at 298 K for 2 h after measuring of the first isotherms (the filled marks). For all the samples, the adsorbed amount of CO_2 during the first isotherm is larger than that during the second isotherms. This suggests that a part of CO_2 adsorbed in the first isotherm are adsorbed irreversibly, because CO_2 molecules reversibly adsorbed are supposed to be desorbed by outgassing before measuring the second isotherm. As seen in Fig. 9 the first and second isotherms above ca. 200 Torr parallel each other. The amount of irreversible adsorption (abbreviated n_i) was evaluated from the difference in the adsorbed amounts of the first and second isotherms above 200 Torr. The obtained n_i values (molecule nm^{-2}) are plotted against X_{Fe} by the open circles in Fig. 10. n_i decreases with an increase of X_{Fe}, which means that the irreversible adsorption sites for CO_2 decrease with Fe(III)-substitution.

Figures 11a and 11b show adsorption isotherms of CH_3OH on pure and Fe(III)-substituted CaHAPs outgassed at 573 K for 2 h. Similarly to CO_2 adsorption, the amount of CH_3OH adsorbed during the first isotherms (the filled marks) is larger than that during the second isotherms (the open marks). The difference in the first and second isotherms is more pro-

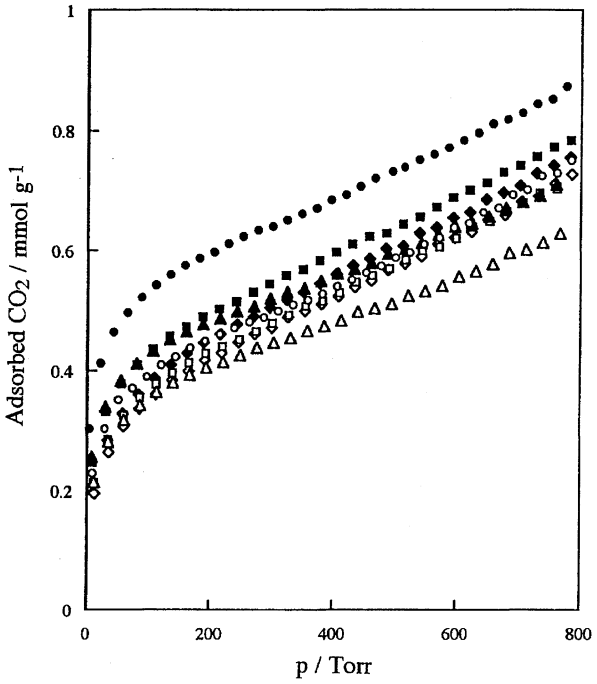

Fig. 9. Adsorption isotherms of CO_2 on CaHAP substituted with Fe^{3+} ions at different X_{Fe}. The first and second isotherms are shown by the filled and open marks, respectively. ●○, X_{Fe}=0; ▲△, X_{Fe}=0.04; ■□, X_{Fe}=0.06; ◆◇, X_{Fe}=0.11.

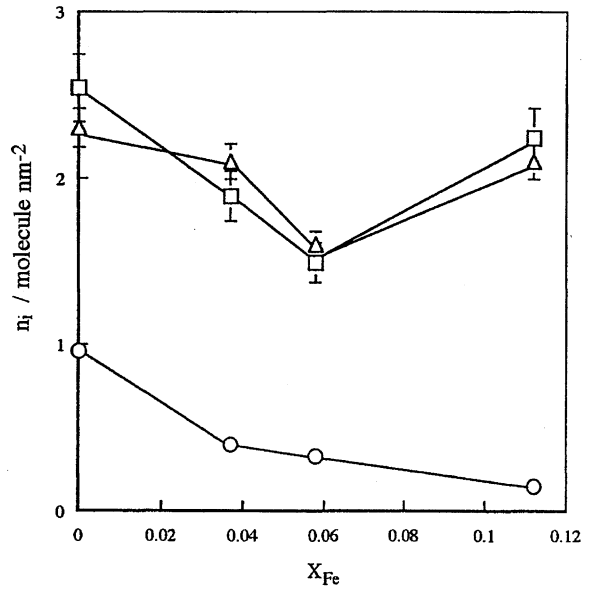

Fig. 10. Amounts of irreversible adsorption (n_i) of CO_2 (○), CH_3OH (□), and H_2O (△) vs. X_{Fe}.

nounced at low relative pressures as shown in Fig. 11b, indicating that the adsorption interaction in the first adsorption is markedly stronger than that in the second adsorption, that is, there are strong adsorption sites for CH_3OH on the CaHAP surface. Dry and Beebe[23] have found that the heat of adsorption of CH_3OH in the first adsorption on CaHAP is considerably larger than that in the second adsorption. They

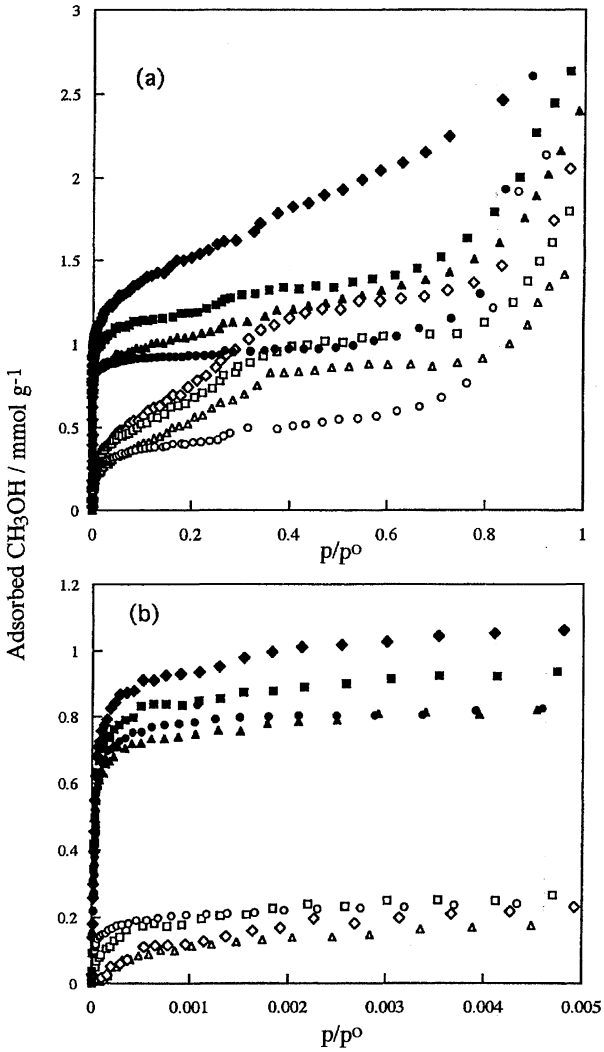

Fig. 11. Adsorption isotherms of CH_3OH on CaHAP substituted with Fe^{3+} ions at different X_{Fe}. The first and second isotherms are shown by the filled and open marks, respectively. The isotherms shown in (b) are low pressure part of the isotherms shown in (a). $p°$ is 112.03 Torr. ●○, X_{Fe}=0; ▲△, X_{Fe}=0.04; ■□, X_{Fe}=0.06; ◆◇, X_{Fe}=0.11.

have explained this fact by assuming that the irreversible adsorption sites for CH_3OH on CaHAP are covered by CH_3 radicals in the first adsorption. The amount of irreversibly adsorbed CH_3OH (n_i) was evaluated from the difference between the BET monolayer adsorption capacities obtained from the first and second adsorption isotherms. n_i is plotted against X_{Fe} by the squares in Fig. 10. n_i decreases with increasing X_{Fe} and then increases at X_{Fe}=0.11, different from CO_2 adsorption.

Figures 12a and 12b compare adsorption isotherms of H_2O on the samples with different X_{Fe} outgassed at 573 K for 2 h. In the same manner for CO_2 and CH_3OH adsorption, the adsorbed amount of H_2O during the second isotherms (the open marks) is less than that during the first ones (the filled marks), indicating irreversible adsorption of H_2O. We estimated the amount of irreversibly adsorbed H_2O (n_i) by

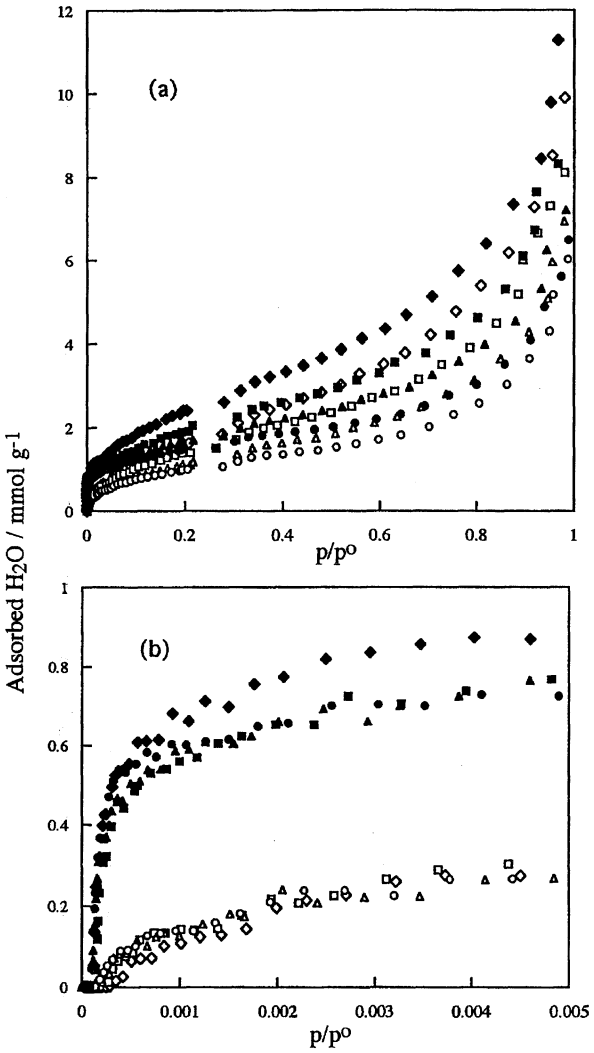

Fig. 12. Adsorption isotherms of H_2O on CaHAP substituted with Fe^{3+} ions at different X_{Fe}. The first and second isotherms are shown by the filled and open marks, respectively. The isotherms shown in (b) are low pressure part of the isotherms shown in (a). $p°$ is 23.76 Torr. ●○, X_{Fe}=0; ▲△, X_{Fe}=0.04; ■□, X_{Fe}=0.06; ◆◇, X_{Fe}=0.11.

the same method for CH_3OH adsorption. The obtained n_i is plotted against X_{Fe} by the triangles in Fig. 10. It should be noted that n_i of H_2O is close to that of CH_3OH, which suggests that the irreversible adsorption sites for H_2O and CH_3OH are the same. As discussed below on the base of in situ FTNIR results, the surface P–OH and Fe–OH groups act as the irreversible adsorption sites for H_2O and CH_3OH. As shown in Figs. 11b and 12b, the first isotherms of CH_3OH at low $p/p°$ rise more steeply compared with those of H_2O, indicating that the adsorption interaction of CH_3OH is stronger than that of H_2O. This may be interpreted by the difference in the irreversible adsorption mechanism of these adsorptives: the irreversible adsorption of CH_3OH takes place by methoxylation of the surface P–OH groups and that of H_2O by hydration of the protons of the surface acidic P–OH groups. The former adsorption interaction is stronger than the latter one.

In situ IR Spectra. IR spectra of the samples adsorbing CO_2 and CH_3OH were taken in situ to examine the adsorption sites for these molecules. Figure 13 shows the spectra of the sample (X_{Fe}=0.11) adsorbing different amounts of CO_2. The amount of adsorbed CO_2 given in this figure was estimated from the first adsorption isotherm on the same sample shown in Fig. 9. As seen in Fig. 13, the bands due to the surface P–OH groups become weak as the amount of adsorbed CO_2 increases. However, we hardly see the change of the surface Fe–OH band at 3707-cm^{-1} with CO_2 adsorption, because of overlap of this band with the 3704-cm^{-1} band due to CO_2 in the gas phase. The band due to adsorbed CO_2 appeared at 2335 cm^{-1} and grew with an increase in the adsorbed amount, though the band is not shown in this figure. When outgassed at 298 K after taking spectrum c, the surface P–OH bands almost recover while the intensity of the surface Fe–OH band is only 28% of the intensity before adsorption (spectrum d). Further outgassing at 573 K revives the surface Fe–OH band up to 44% of the initial intensity (spectrum e). The weak 2335-cm^{-1} band due to the adsorbed CO_2 was still detected after this outgassing. These findings prove that the surface P–OH groups act as the reversible adsorption sites for CO_2 and the surface Fe–OH groups function both the reversible and irreversible sites. However, pure CaHAP with no surface Fe–OH groups adsorbed CO_2 irreversibly and n_i decreased with Fe(III)-substitution (Fig. 10). n_i of the material (X_{Fe}=0.11) slightly decreased from 0.17

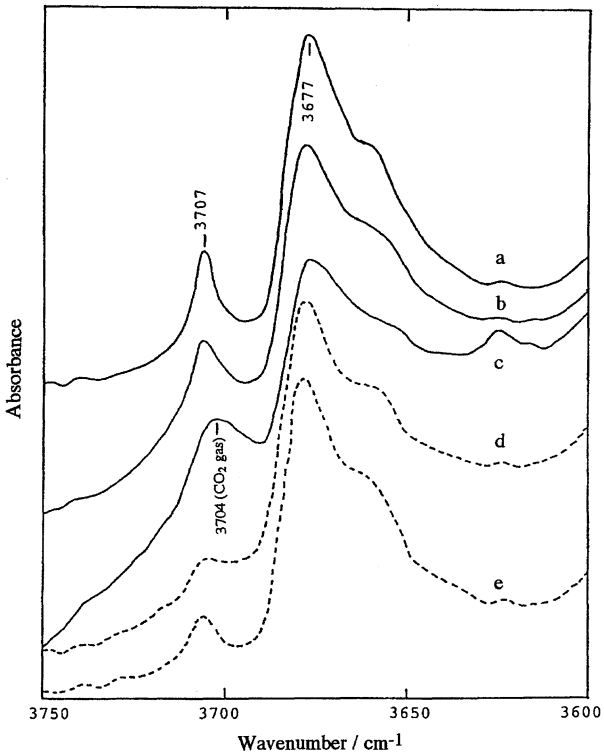

Fig. 13. Change of IR spectra of Fe(III)-substituted CaHAP (X_{Fe}=0.11) by CO_2 adsorption. (a) before adsorption, (b) 0.62 molecule nm^{-2}, (c) 1.57 molecule nm^{-2}, (d) outgassed at 298 K after taking spectrum c, (e) outgassed at 573 K after taking spectrum d.

to 0.15 molecule nm^{-2} on outgassing at 673 K, where the surface Fe–OH groups were completely removed. Hence there seem to be other kinds of irreversible adsorption sites for CO_2 in addition to the surface Fe–OH groups. To know the detailed adsorption mechanism of CO_2 the IR spectra at wavenumbers below 2000 cm^{-1} are required. However, a low transparency of the CaHAP samples to IR beam did not allow us to take the spectra below 2000 cm^{-1}.

Figure 14 depicts the change of the spectra of the material (X_{Fe}=0.11) with CH_3OH adsorption. The amount of adsorbed CH_3OH was estimated from the first isotherm of CH_3OH in Fig. 11. All the bands due to the surface P–OH and Fe–OH groups diminish by CH_3OH adsorption and completely disappeared in spectrum c. The bands due to CH_3 groups appeared at 2955, 2840, and 2820 cm^{-1} and their intensities increased with an increase in the amount of adsorbed CH_3OH, although the spectra below 3600 cm^{-1} are not shown here. When outgassed at 298 K after taking spectrum c, the surface OH bands are essentially not detected (spectrum d). After further evacuation at 573 K the surface P–OH bands are partially restored whereas the Fe–OH band remains almost absent (spectrum e). The bands due to CH_3 groups were still observed at 2955 and 2850 cm^{-1} after this outgassing at 573 K. We can conclude therefore that both the surface P–OH and Fe–OH groups are the irreversible adsorption sites for CH_3OH and the latter groups are stronger adsorption sites than the former ones.

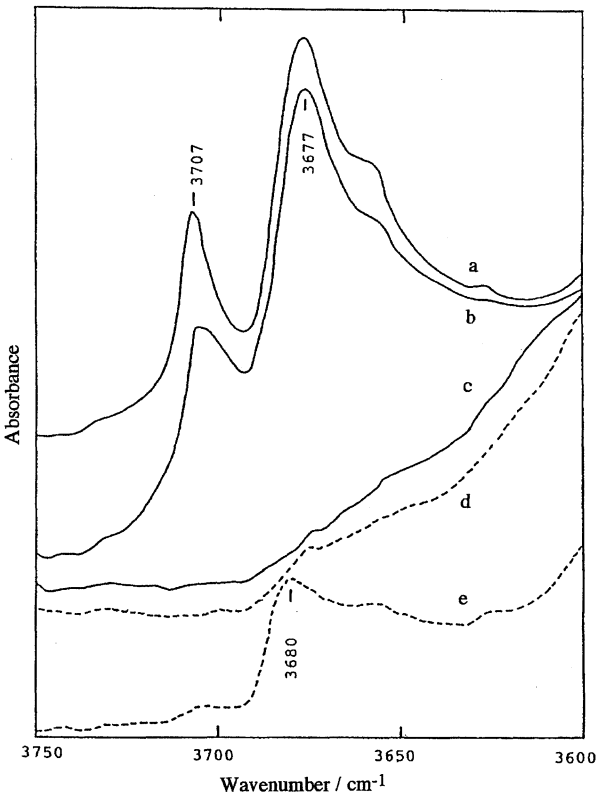

Fig. 14. Change of IR spectra of Fe(III)-substituted CaHAP (X_{Fe}=0.11) by CH_3OH adsorption. (a) before adsorption, (b) 2.2 molecule nm^{-2}, (c) 4.2 molecule nm^{-2}, (d) outgassed at 298 K after taking spectrum c, (e) outgassed at 573 K after taking spectrum d.

Adsorption Sites for CO_2, CH_3OH, and H_2O. We can infer from the structure of the predominant crystal faces of CaHAP[24,25] that possible surface ions are PO_4^{3-}, HPO_4^{2-}, OH^-, and Ca^{2+} ions. The Ca^{2+} ions may be covered by OH^- ions and/or H_2O molecules, because the CaHAP samples used in this study were synthesized in an aqueous system. It has been confirmed by the FTNIR method that H_2O molecules strongly bonded to the surface Ca^{2+} ions are removed by outgassing at a temperature range from ca. 400 to ca. 800 K.[11] Therefore, there is a possibility that the Ca^{2+} ions exposed by pretreating at 573 K act as the irreversible adsorption sites for all adsorptives. However, no experimental evidence is available for this because the analysis of the exposed Ca^{2+} ions is difficult at the moment.

FTNIR results reveal that the surface P–OH groups are the reversible adsorption sites for CO_2 and the irreversible adsorption sites for CH_3OH and H_2O. IR bands due to CH_3 groups appeared even after outgassing the CH_3OH-adsorbed samples above 573 K. Therefore the strong irreversible adsorption of CH_3OH would take place via methoxylation of the surface P–OH and Fe–OH groups. The total absorbance of all the surface P–OH bands, which was estimated by dividing the area intensity of the surface P–OH bands by the specific surface area of the samples, increased from 0.34 to 0.40 (in arbitrary units) with increasing X_{Fe} from 0 to 0.11. Nevertheless, n_i of H_2O and CH_3OH first decreased and then increased as X_{Fe} increased (Fig. 10). This may be accounted for by an assumption that Fe(III)-substitution decreases the surface Ca^{2+} ions acting as irreversible adsorption sites for H_2O and CH_3OH, but increases the surface P–OH groups which are irreversible adsorption sites for these adsorptives. This leads to a minimum of n_i of H_2O and CH_3OH.

The surface OH^- ions binding to Ca^{2+} ions would function the irreversible adsorption sites for CO_2 via a reaction such as $CO_2+OH^- \rightarrow HCO_3^-$. These OH^- ions decrease owing to the decrease of Ca^{2+} ions with Fe(III)-substitution, so that n_i of CO_2 decreases as X_{Fe} increases (Fig. 10). However, the surface OH^- ions could not be detected by the FTNIR method. It has been reported that the OH^- ions of CaHAP are hydrogen-bonded to O atoms of the neighboring PO_4^{3-} ions.[26] Thus, the IR bands due to the stretching mode of the surface OH^- ions seem to overlap or close to the strong band of bulk OH^- ions at 3572 cm^{-1}.

The surface Fe–OH groups function strong irreversible adsorption sites for all of the adsorptives. As presumed from Table 1, the concentration of the surface Fe–OH groups is not so high as to have a marked influence on n_i of these adsorptives. A more quantitative discussion on the adsorption sites is difficult unless a method is developed to determine the precise surface composition of CaHAP.

The authors thank Mr. Masao Fukusumi of Osaka Municipal Technical Research Institute for his help with TEM measurements. This study was supported in part by Nippon Sheet Glass Foundation for Materials Science and Technol-

ogy and the Grants-in-Aids for Science Research Fund (B) and (C) of the Ministry of Education, Science, Sports and Culture.

References

1) J. C. Elliott, "Structure and Chemistry of the Apatites and Other Calcium Orthophosphates," Elsevier, Amsterdam (1994), p. 111.
2) Y. Tanizawa, K. Sawamura, and T. Suzuki, *J. Chem. Soc., Faraday Trans.*, **86**, 4025 (1990).
3) Y. Tanizawa, K. Sawamura, and T. Suzuki, *J. Chem. Soc., Faraday Trans.*, **86**, 1071 (1990).
4) T. Suzuki, K. Ishigaki, and M. Miyake, *J. Chem. Soc., Faraday Trans.*, **80**, 3157 (1984).
5) T. Suzuki, T. Hatsushika, and M. Miyake, *J. Chem. Soc., Faraday Trans.*, **78**, 3605 (1982).
6) T. Suzuki, T. Hatsushika, and Y. Hayakawa, *J. Chem. Soc., Faraday Trans.*, **77**, 1059 (1981).
7) R. M. H. Verbeeck, C. J. Lassuyt, H. J. M. Heijligers, F. C. M. Driessens, and J. W. G. A. Vralijk, *Calcif. Tissue Int.*, **33**, 243 (1981).
8) H. J. M. Heijligers, F. C. M. Driessens, and R. M. H. Verbeeck, *Calcif. Tissue Int.*, **29**, 127 (1979).
9) M. Misono and W. K. Hall, *J. Phys. Chem.*, **77**, 791 (1973).
10) Y. Matsumura, J. B. Moffat, S. Sugiyama, H. Hayashi, N. Shigemoto, and K. Saitoh, *J. Chem. Soc., Faraday Trans.*, **90**, 2133 (1994).
11) T. Ishikawa, M. Wakamura, and S. Kondo, *Langmuir*, **5**, 140 (1989).
12) T. Ishikawa, M. Wakamura, T. Kawase, and S. Kondo, *Langmuir*, **7**, 596 (1991).
13) T. Ishikawa, and S. Kondo, "Fundamentals of Adsorption," ed by A. B. Mersman and S. E. Scholl, Engineering Foundation, New York (1991), p. 231.
14) T. Ishikawa, "Adsorption on New and Modified Inorganic Sorbents," ed by A. Dabrowski and V. A. Tertykh, Elsevier, Amsterdam (1996), p. 301.
15) T. Ishikawa, H. Saito, and K. Kandori, *J. Chem. Soc., Faraday Trans.*, **88**, 2937 (1992).
16) T. Ishikawa, H. Saito, A. Yasukawa, and K. Kandori, *J. Chem. Soc., Faraday Trans.*, **89**, 3821 (1993).
17) D. F. Boltz and M. G. Mellon, *Anal. Chem.*, **20**, 749 (1948).
18) B. C. Lippens and J. H. de Boer, *J. Catal.*, **4**, 319 (1965).
19) H. S. Mcintyre and D. G. Zetaruk, *Anal. Chem.*, **49**, 1521 (1977).
20) E. E. Berry, *J. Inorg. Nucl. Chem.*, **29**, 1585 (1967).
21) H. Monma, S. Ueno, and T. Kanazawa, *J. Chem. Technol. Biotechnol.*, **31**, 15 (1981).
22) T. Ishikawa, S. Nitta, and S. Kondo, *J. Chem. Soc., Faraday Trans. 1*, **82**, 2401 (1986).
23) M. E. Dry and R. A. Beebe, *J. Phys. Chem.*, **64**, 1300 (1960).
24) M. I. Kay and R. A. Young, *Nature*, **204**, 1050 (1964).
25) K. Sudarsanan and R. A. Young, *Acta Crystallogr., Sect. B*, **B25**, 1534 (1969).
26) C. B. Baddiel and E. E. Berry, *Spectrochim. Acta*, **22**, 1407 (1966).